Supporting Information for

The Two-Dimensional Functionalized MBenes Mg_2B_3T (T=O, H, and F) Monolayers as Anode Material for High-Performance K-ion Batteries

Fengzhang Tang,[a] Jiafei Pang,[a] Jinni Yang,[b] Xiaoyu Kuang[a]* and Aijie Mao[a]*

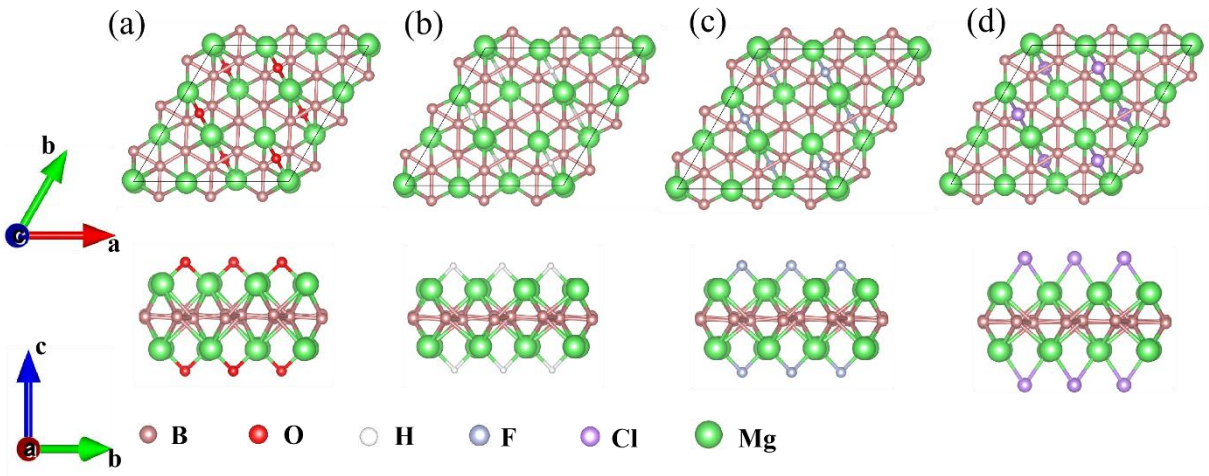

Fig. S1 Top and side view of Mg_2B_3T (T=O, H, F, and Cl) monolayer. Here, (a) Mg_2B_3O, (b) Mg_2B_3H, (c) Mg_2B_3F, and (d) Mg_2B_3Cl; The B and Mg atoms are labeled pink and green balls, while the O, H, F and Cl atoms are labeled by red, white, light blue and purple respectively.

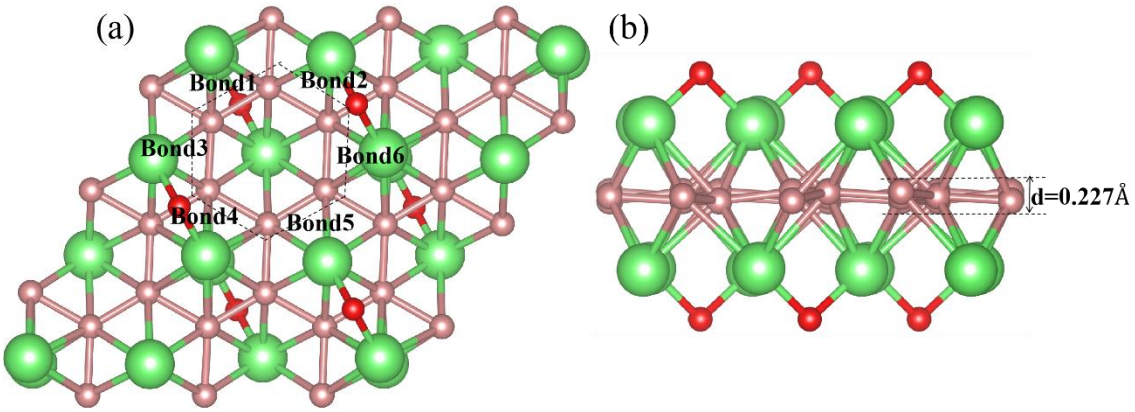

Fig. S2 (a) Six B-B bonds of the boron ring in the Mg_2B_3O monolayer, and (b) fold height diagram of the intermediate boron layer.

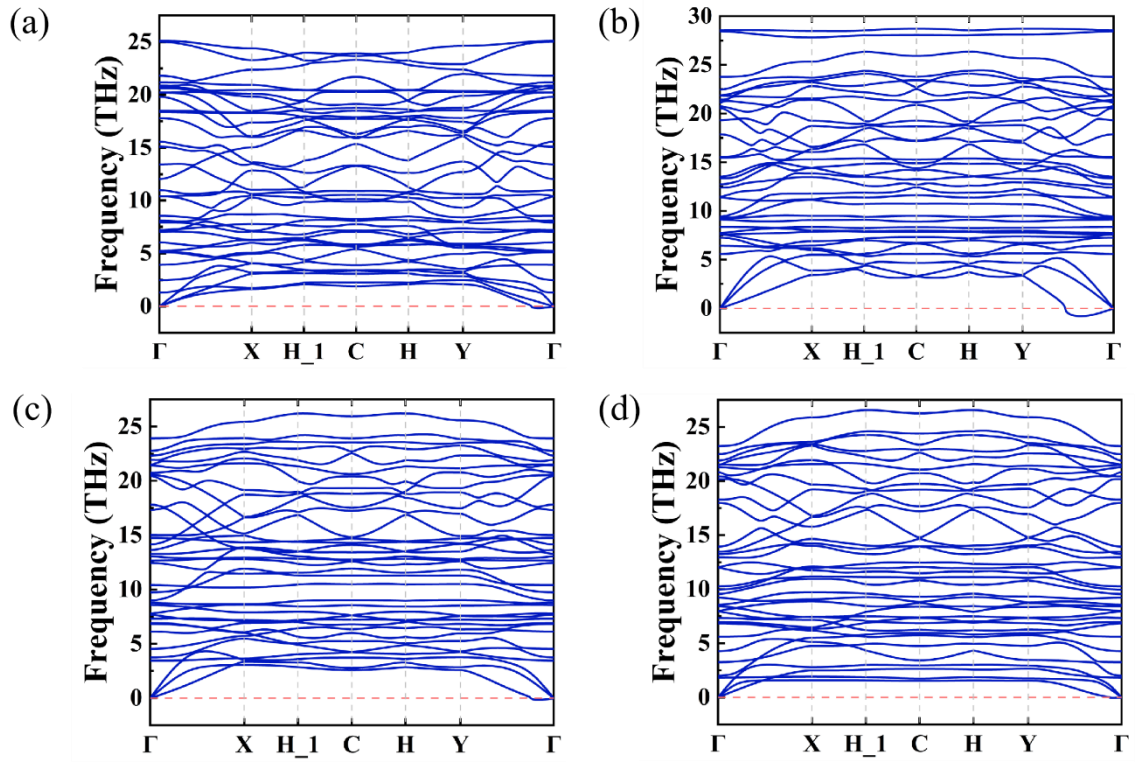

Fig. S3 The phonon dispersions curves for the (a) Mg_2B_3O monolayer, (b) Mg_2B_3H monolayer, (c) Mg_2B_3F monolayer, and (d) Mg_2B_3Cl monolayer, respectively.

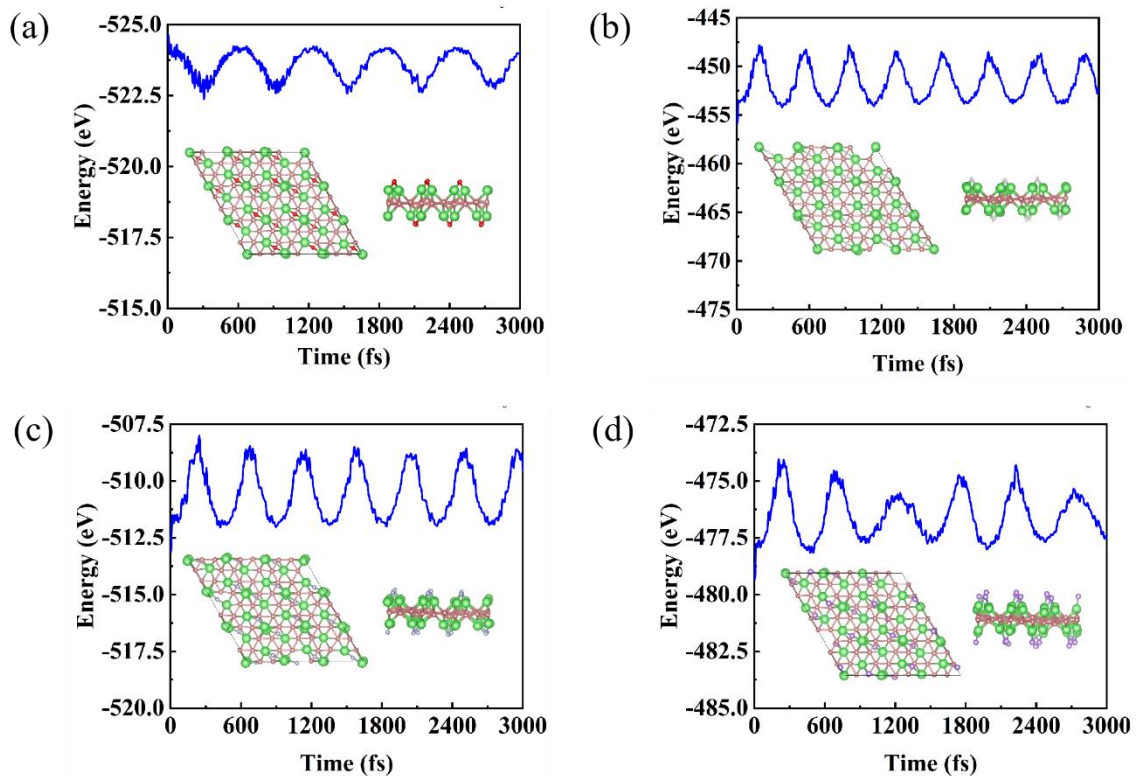

Fig. S4 Structural energy fluctuations and electron snapshots simulated by AIMD at 300K: (b) Mg_2B_3H monolayer, (c) Mg_2B_3F monolayer, and (d) Mg_2B_3Cl monolayer, respectively; while (a) Mg_2B_3O monolayer is thermodynamically stable at 100K.

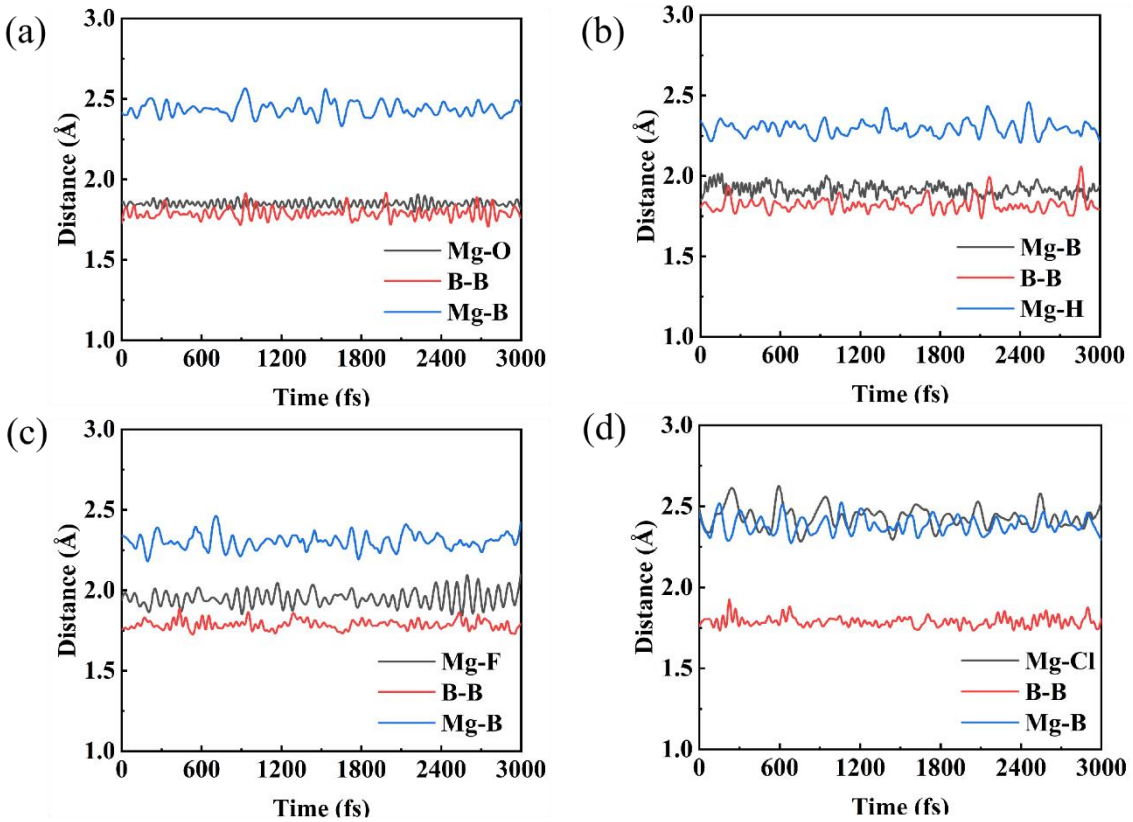

Fig. S5 Changes in bond lengths within the structures of (a) Mg_2B_3O monolayer, (b) Mg_2B_3H monolayer, (c) Mg_2B_3F monolayer, and (d) Mg_2B_3Cl monolayer during AIMD simulations.

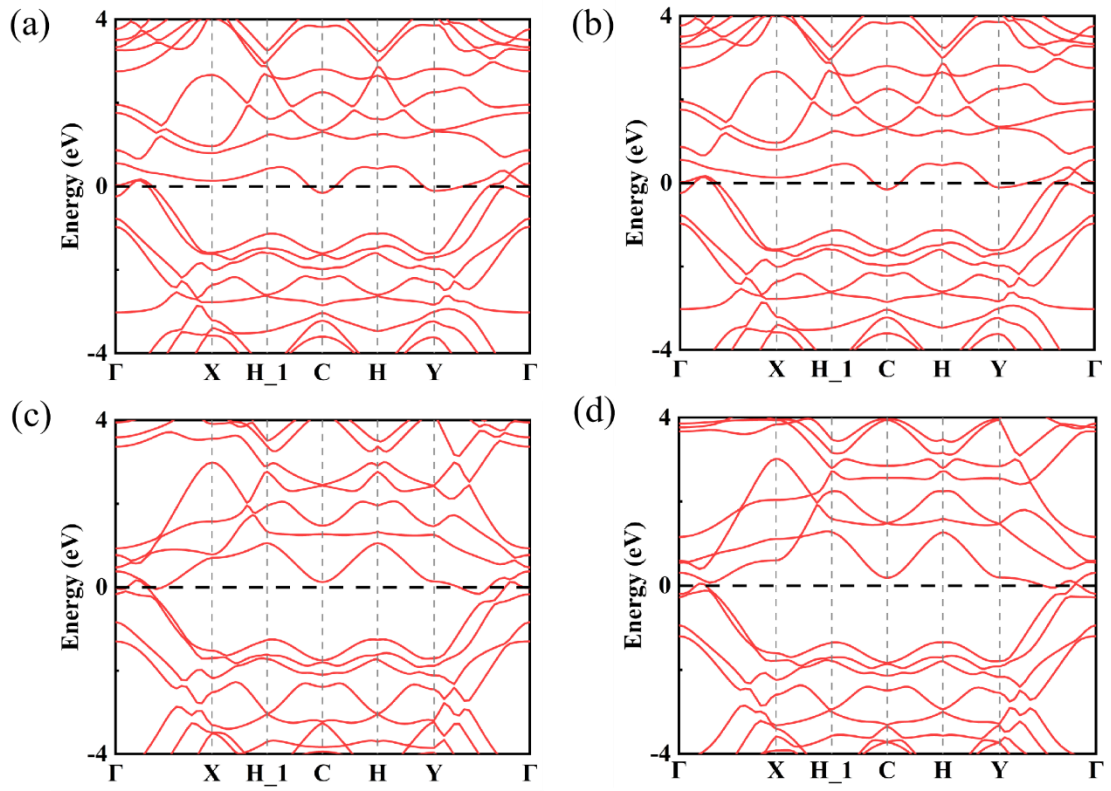

Fig. S6 The electronic band structures for the (a) Mg_2B_3O monolayer, (b) Mg_2B_3H monolayer, (c) Mg_2B_3F monolayer, and (d) Mg_2B_3Cl monolayer, respectively.

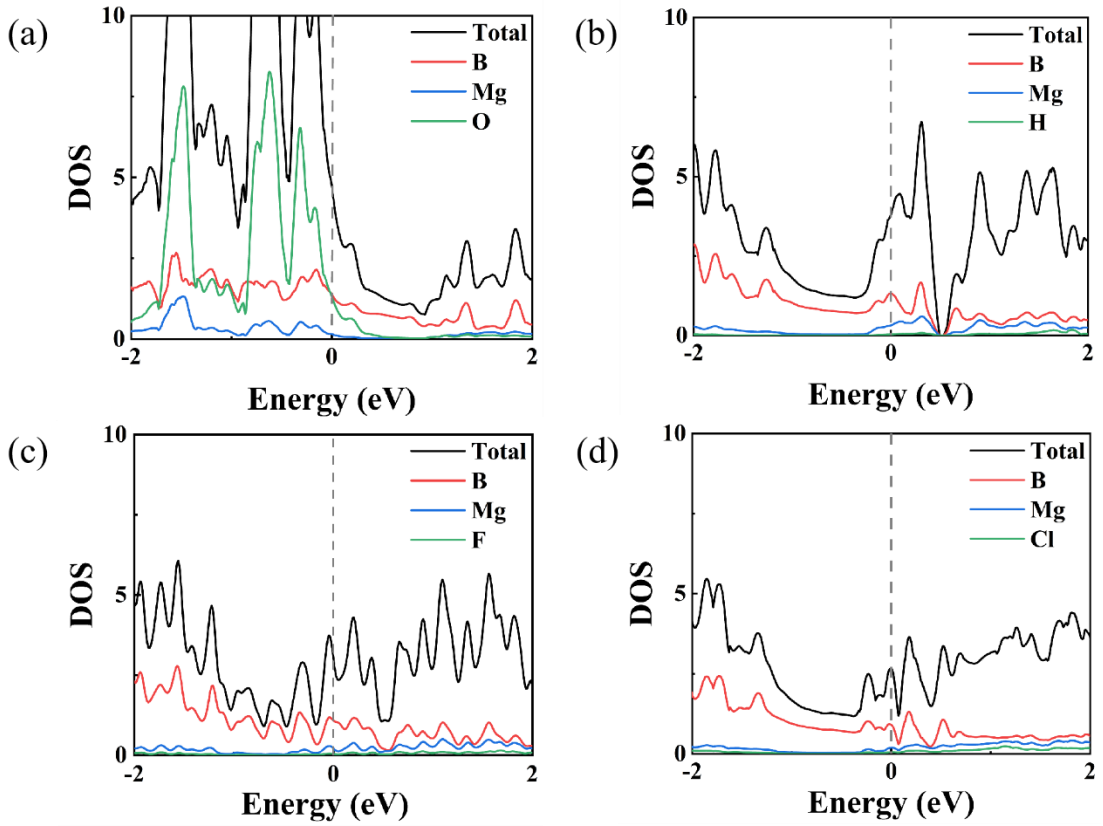

Fig. S7 The calculated partial density of states (DOS) for the (a) Mg_2B_3O monolayer, (b) Mg_2B_3H monolayer, (c) Mg_2B_3F monolayer, and (d) Mg_2B_3Cl monolayer, respectively.

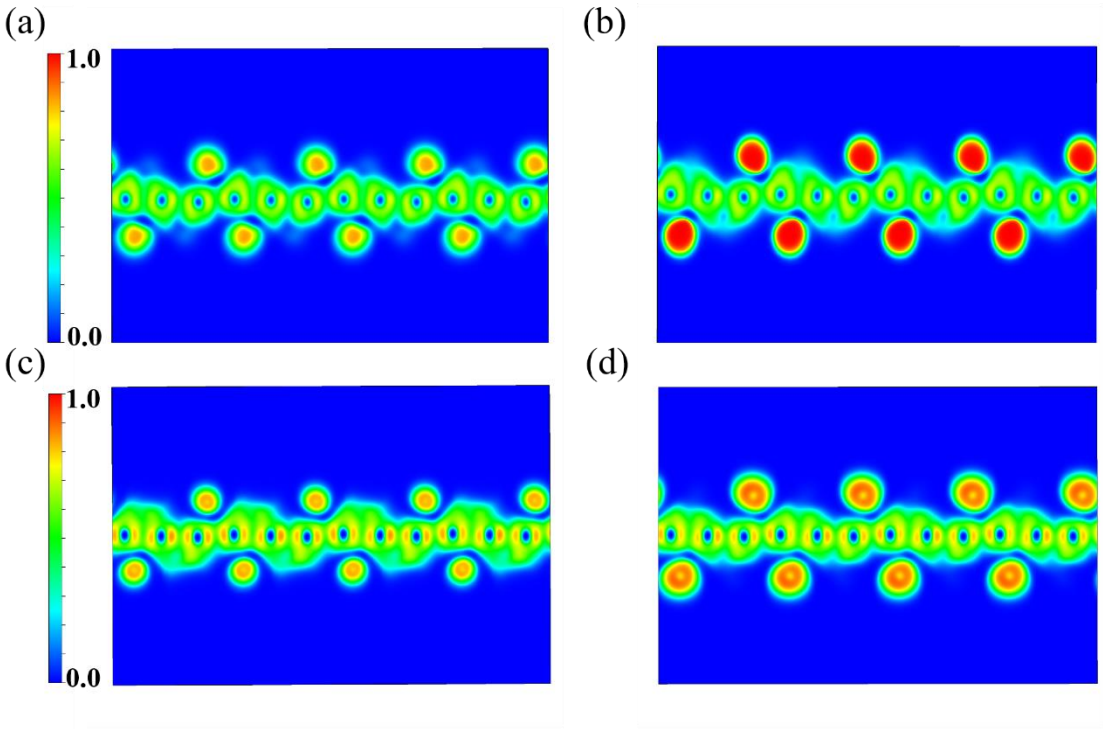

Fig. S8 The electron localization function (ELF) for the (a) Mg_2B_3O monolayer, (b) Mg_2B_3H monolayer, (c) Mg_2B_3F monolayer, and (d) Mg_2B_3Cl monolayer, respectively.

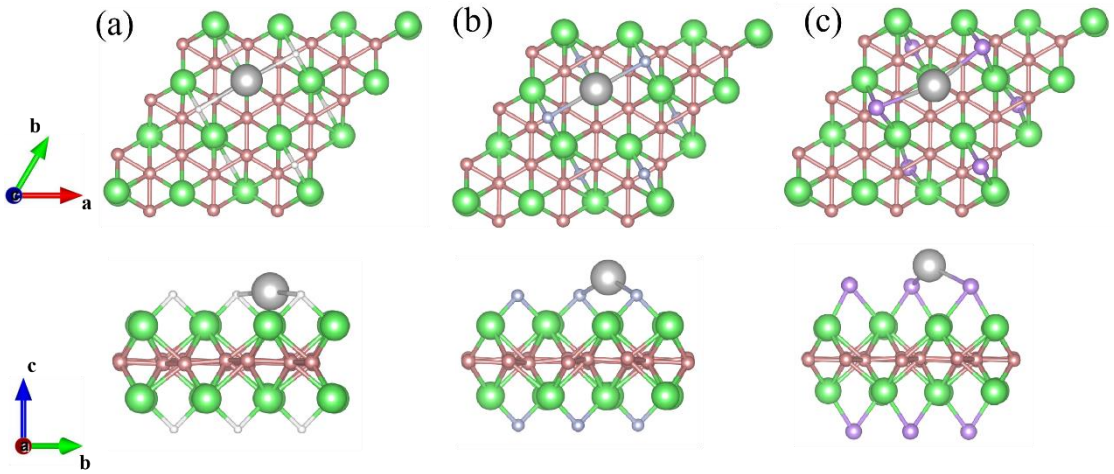

$E_{ad} = -0.29\ eV$ $E_{ad} = -0.72\ eV$ $E_{ad} = -0.54\ eV$

Fig. S9 The top view and side view of single K atom adsorbed on (a) Mg_2B_3H monolayer, (b) Mg_2B_3F monolayer, and (c) Mg_2B_3Cl monolayer structure and the corresponding adsorption energy. The silver ball represents the K atom.

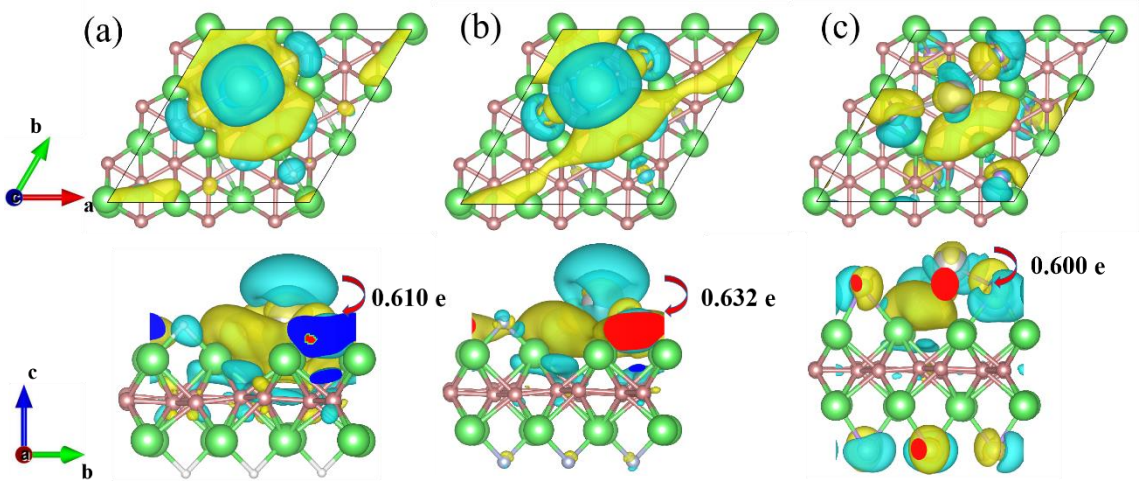

Fig. S10 Top view and side view of charge density difference diagram of K adsorption at the A4 site of (a) Mg_2B_3H monolayer, (b) Mg_2B_3F monolayer, and (c) Mg_2B_3Cl monolayer. The cyan region indicates a decrease in charge density and the yellow region indicates an increase in charge density.

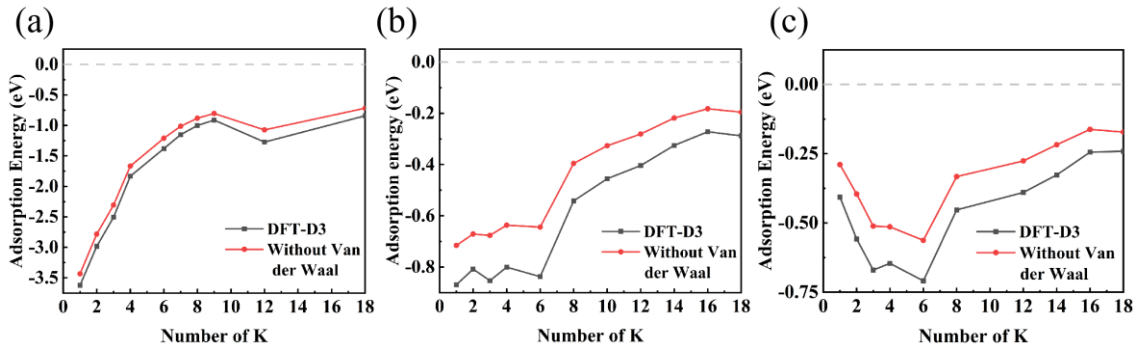

Fig. S11 The adsorption energies of (a)Mg_2B_3O, (b)Mg_2B_3F, and (c)Mg_2B_3H monolayer at different K adsorption concentrations, where the red line indicates the adsorption energies without considering van der Waals interactions, and the black line represents the adsorption energies with Grimme's DFT-D3 considered in VASP.

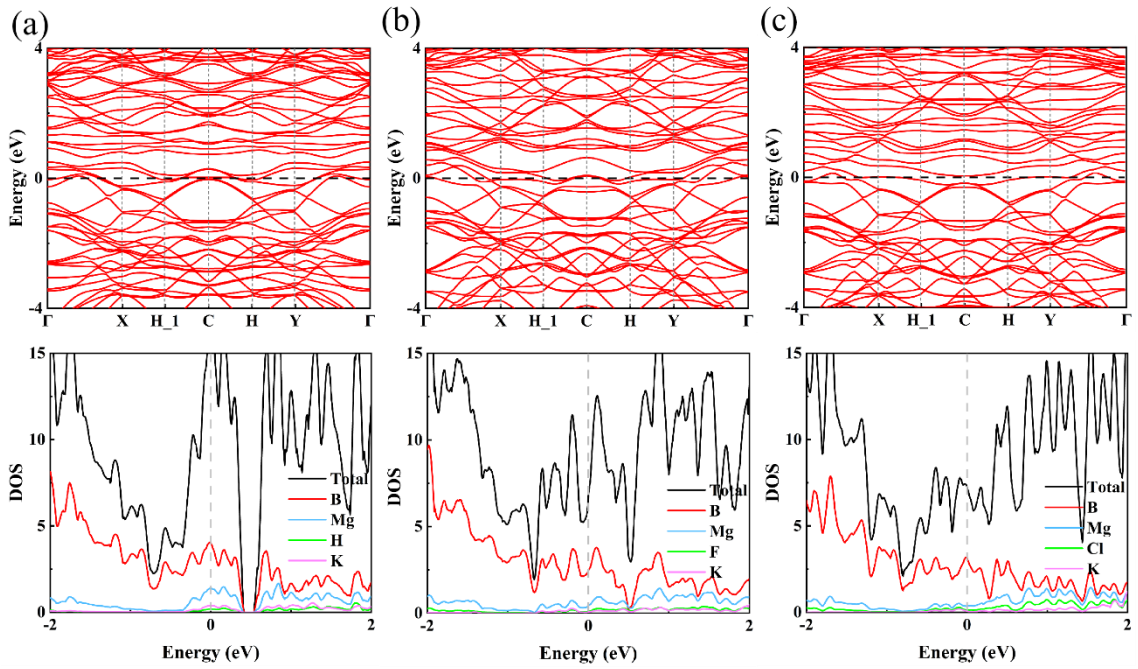

Fig. S12 Electronic band structure and partial density of states (DOS) of (a) Mg_2B_3H monolayer, (b) Mg_2B_3F monolayer, and (c) Mg_2B_3Cl monolayer， respectively.

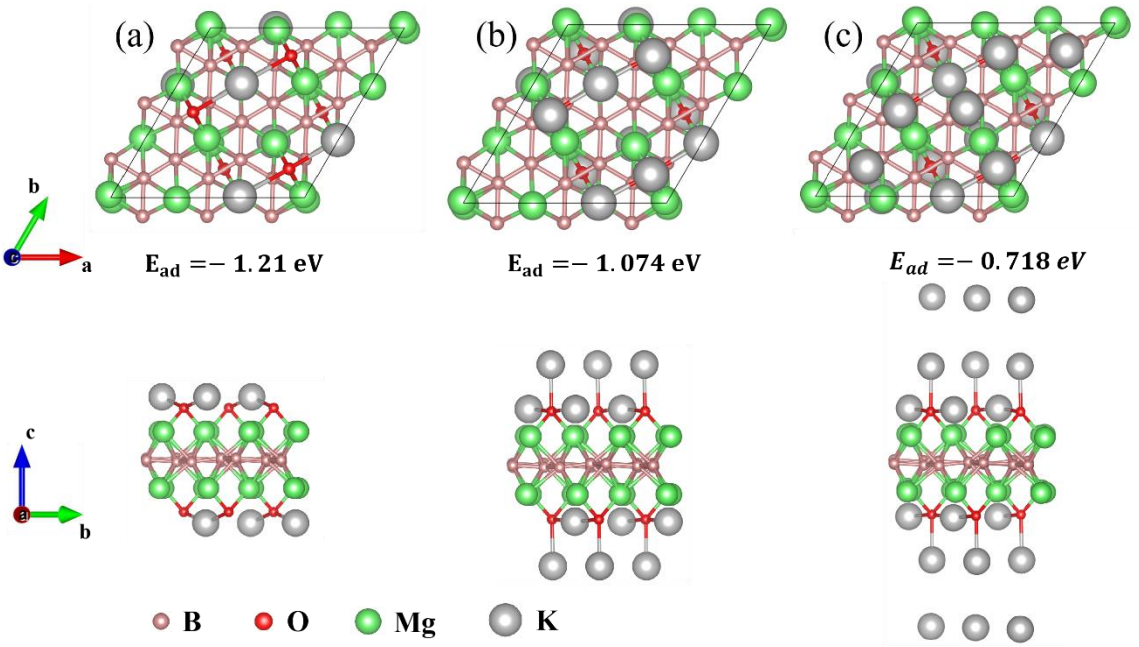

Fig. S13 (a-c) are the top view and side view after adsorption of one, two and three layers of K atoms on both sides of Mg_2B_3O monolayer, respectively.

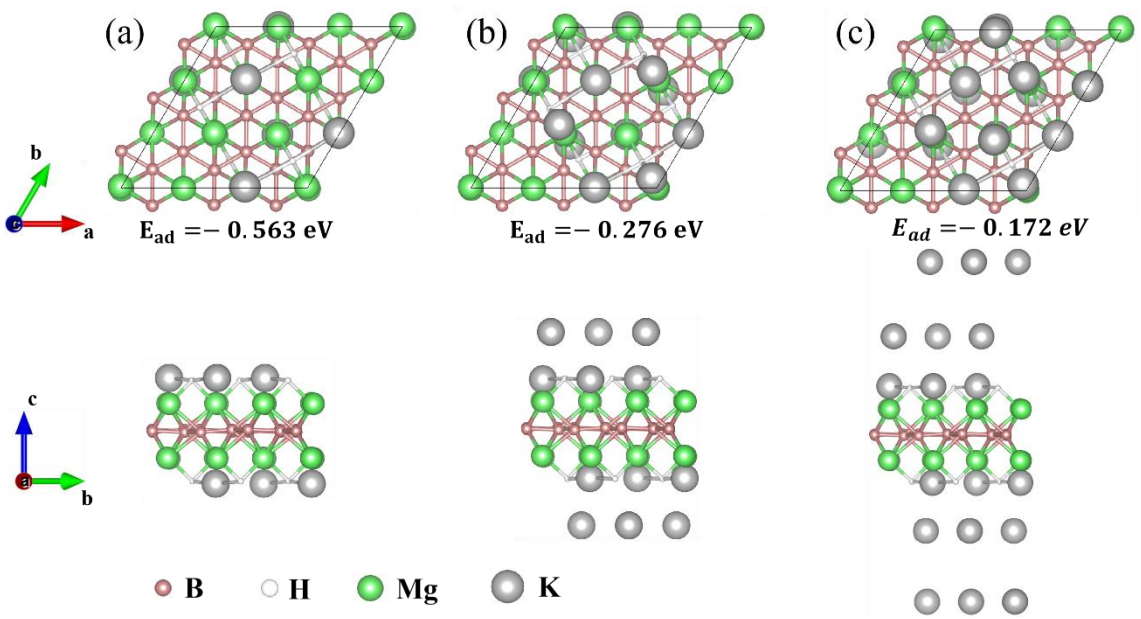

Fig. S14 (a) -(c) are the top view and side view after adsorption of one, two and three layers of K atoms on both sides of Mg_2B_3H monolayer, respectively.

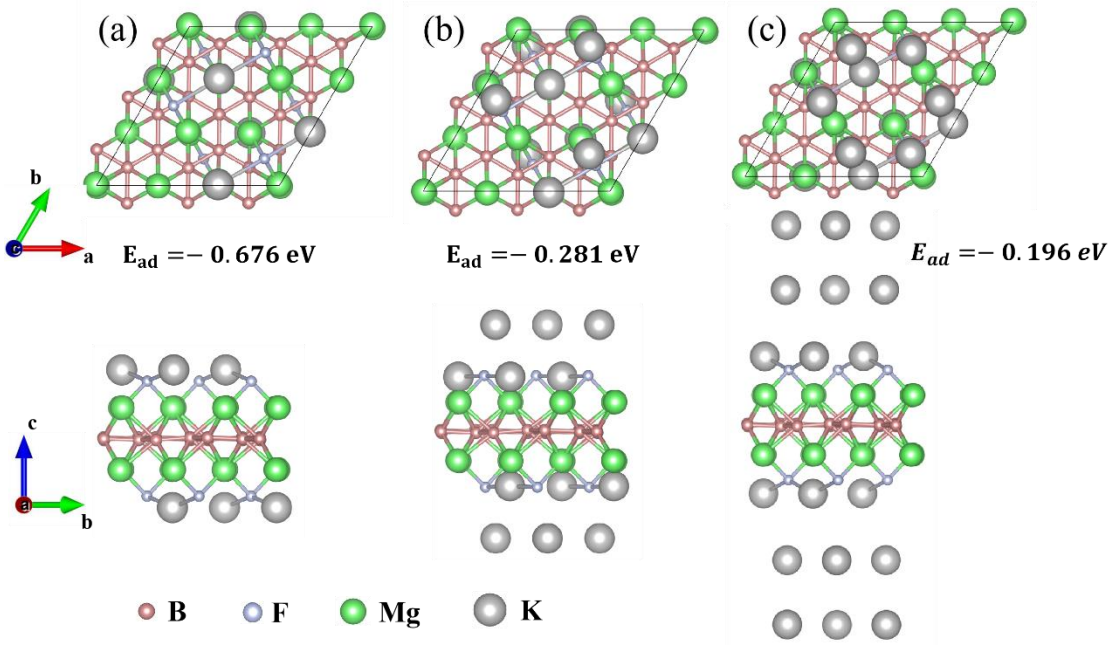

Fig. S15 (a) -(c) are the top view and side view after adsorption of one, two and three layers of K atoms on both sides of Mg_2B_3F monolayer, respectively.

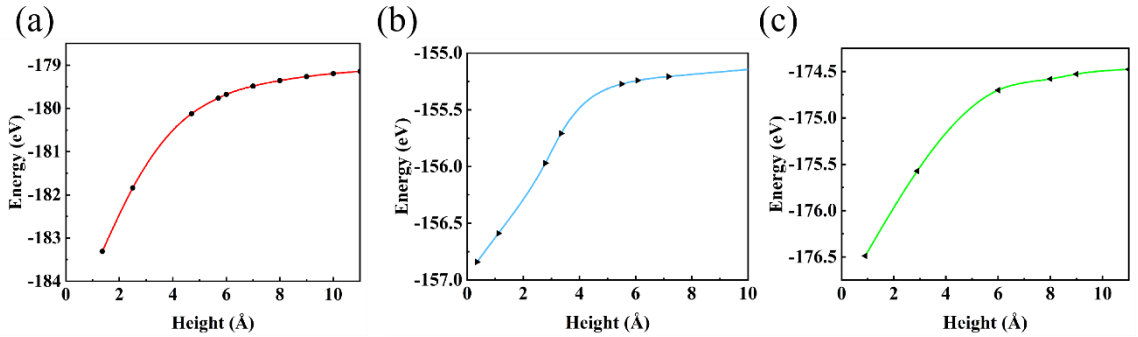

Fig. S16 Total energy of metals on (a) Mg_2B_3O, (b) Mg_2B_3H and (c) Mg_2B_3F as a function of the height from metal to Mg_2B_3T surface.

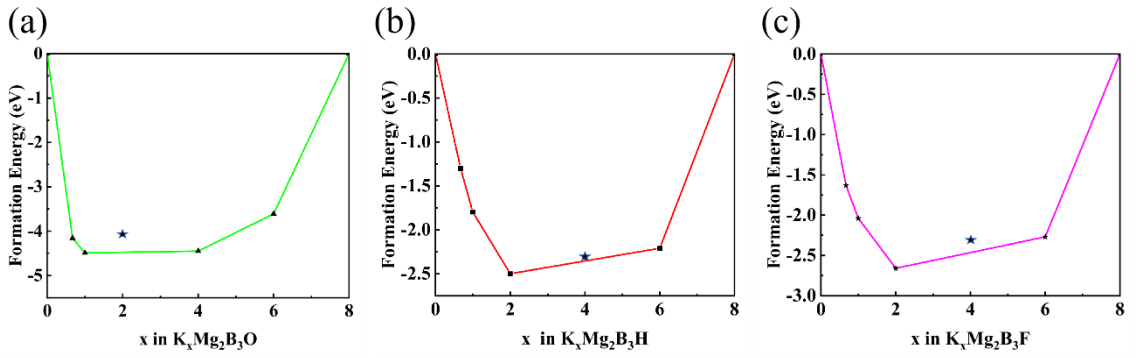

Fig. S17 The formation energies of (a) $K_xMg_2B_3O$, (b) $K_xMg_2B_3H$ and (c) $K_xMg_2B_3F$. The intermediate phase corresponding to the data points on the real line of the convex hull is thermodynamically stable.

	B-B（Å）[Mg_2B_3O]	B-B （Å）[Mg_2B_3H]	B-B （Å）[Mg_2B_3F]	B-B （Å）[Mg_2B_3Cl]
Bond1	1.709	1.800	1.774	1.792
Bond2	1.768	1.762	1.762	1.769
Bond3	1.774	1.771	1.777	1.782
Bond4	1.769	1.784	1.786	1.796
Bond5	1.718	1.765	1.750	1.772
Bond6	1.718	1.789	1.798	1.806

Tab. S1 The lengths of each B-B bond in the boron hexagonal rings of the Mg_2B_3T (T=O, H, F, and Cl) monolayers.

	C_{11} (GPa)	C_{12} (GPa)	C_{22} (GPa)	C_{16} (GPa)	C_{26} (GPa)	C_{66} (GPa)
Mg_2B_3O	453.43	118.96	443.17	37.34	-80.99	54.70
Mg_2B_3H	546.68	20.98	505.11	-45.66	-19.58	240.99
Mg_2B_3F	549.76	38.90	523.27	-6.25	-1.34	259.38
Mg_2B_3Cl	569.82	18.34	479.05	-28.43	-34.33	251.63

Tab. S2 Elastic constant of Mg_2B_3T (T=O, H, F, and Cl) monolayer.

		B	Mg	O	K
Charge transfer(e)	**K@Mg_2B_3O**	+7.610	-14.689	+7.866	-0.787
	Mg_2B_3O	+4.235	-10.166	+5.893	
		B	**Mg**	**H**	**K**
	K@Mg_2B_3H	+8.640	-12.990	+3.961	-0.610
	Mg_2B_3H	+5.406	-9.897	+3.491	
		B	**Mg**	**F**	**K**
	K@Mg_2B_3F	+8.803	-13.670	+5.531	-0.632
	Mg_2B_3F	+5.373	-9.872	+4.499	

Tab. S3 The charge transfer between the Mg_2B_3T(T=O, H and F) monolayer with and without K (where "+" indicates a gain in charge, and "-" indicates a loss of charge).

	Number of K atoms	a(Å)	b(Å)	Volume variation(%)
Mg_2B_3O	0	9.017	9.154	0
	6	9.200	9.221	0.015
	12	9.406	9.393	0.113
	18	9.367	9.356	0.086
Mg_2B_3H	0	9.309	9.262	0
	6	9.430	9.448	0.036
	12	9.434	9.454	0.038
	18	9.367	9.391	0.016
Mg_2B_3F	0	9.197	9.268	0
	6	9.268	9.321	0.004
	12	9.478	9.478	0.052
	18	9.225	9.252	0

Tab. S4 Changes in the in-plane lattice constants and overall volume of the Mg_2B_3T (T=O, H, F) monolayers after adsorbing one, two, and three layers of K atoms.

	$Mg_{12}B_{18}O_6$	K6@$Mg_{12}B_{18}O_6$	K12@$Mg_{12}B_{18}O_6$	K18@$Mg_{12}B_{18}O_6$
Charge transfer(e)	0	4.598	4.3636	4.3757
	$Mg_{12}B_{18}H_6$	K6@$Mg_{12}B_{18}H_6$	K12@$Mg_{12}B_{18}H_6$	K18@$Mg_{12}B_{18}H_6$
Charge transfer(e)	0	4.295	3.714	3.5144
	$Mg_{12}B_{18}F_6$	K6@$Mg_{12}B_{18}F_6$	K12@$Mg_{12}B_{18}F_6$	K18@$Mg_{12}B_{18}F_6$
Charge transfer(e)	0	4.087	3.698	2.924

Tab. S5 Charge transfer value of Mg_2B_3T (T=O, H, F) monolayers after adsorption of K atoms.